Journal of
Marine Science and Engineering

MDPI

Article

Toward an Astrochronology-Based Age-Model for a Messinian Pre-Evaporitic Succession: The Example of Torrente Vaccarizzo Section in Sicily (Italy)

Rosanna Maniscalco [1], Martina Forzese [1,*], Viviana Barbagallo [1], Laura Borzì [1], Natale Maria D'Andrea [1], Salvatore Distefano [1], Chiara Giustolisi [1], Ádam Nádudvari [2], Alessandra Giovanna Pellegrino [1], Luca Maria Foresi [3] and Agata Di Stefano [1]

[1] Dipartimento di Scienze Biologiche, Geologiche ed Ambientali, Università degli Studi di Catania, Corso Italia 57, 95129 Catania, Italy; rosanna.maniscalco@unict.it (R.M.)
[2] Faculty of Natural Sciences, University of Silesia, 60 Będzińska Street, 41-200 Sosnowiec, Poland
[3] Dipartimento di Scienze Fisiche, della Terra e dell'Ambiente, Università degli Studi di Siena, Via Laterina 8, 53100 Siena, Italy
* Correspondence: martina.forzese@phd.unict.it or martina.forzese@gmail.com

Abstract: Tectonic, paleoenvironmental, and paleoclimatic unstable conditions preceding the onset of the Messinian Salinity Crisis (MSC) highly affected marine life. Changes in calcareous plankton association are overall registered in the Mediterranean. They consist of a general transition from abundant and well-diversified planktonic associations to strictly oligotypic assemblages that precede their total disappearance at the onset of evaporitic precipitation. In this work, an accurate quantitative analysis of calcareous plankton, both foraminifers and nannofossils, has been carried out in the Torrente Vaccarizzo Section of Sicily (southern Italy). The aim is to independently define a chronostratigraphic pattern of bioevents preceding the MSC in the absence of magnetostratigraphic or radiometric constraints. The fluctuating abundance of the genus *Orbulina* fits well with the 100 ky Eccentricity maxima, and it is successfully applied to build an astronomically calibrated age-model for the section. On this basis, all the biohorizons have been recalibrated and discussed with regard to the previous literature. Abundant influxes of selected species demonstrated to be of local significance since they are highly affected by paleoenvironmental and paleoclimatic conditions. A chronological sequence of foraminifer and nannofossil events marks the onset of the MSC with a derived age of 5.957 My, which agrees well with previous findings from other Mediterranean sections. This methodology and the new biostratigraphic events may be useful for future studies on pre-evaporitic successions of the Mediterranean.

Keywords: pre-evaporitic deposits; Messinian Salinity Crisis; calcareous plankton; cyclicity

check for updates

Citation: Maniscalco, R.; Forzese, M.; Barbagallo, V.; Borzì, L.; D'Andrea, N.M.; Distefano, S.; Giustolisi, C.; Nádudvari, Á.; Pellegrino, A.G.; Foresi, L.M.; et al. Toward an Astrochronology-Based Age-Model for a Messinian Pre-Evaporitic Succession: The Example of Torrente Vaccarizzo Section in Sicily (Italy). *J. Mar. Sci. Eng.* **2023**, *11*, 915. https://doi.org/10.3390/jmse11050915

Academic Editor: Assimina Antonarakou

Received: 31 March 2023
Revised: 22 April 2023
Accepted: 23 April 2023
Published: 25 April 2023

1. Introduction

Several studies have already been performed on pre-evaporitic deposits (e.g., Tripoli Formation in Sicily, Italy) to understand the complex climatic and tectonic events that preceded the Messinian Salinity Crisis (MSC) in the Mediterranean. According to the wider literature available so far, the pre-evaporitic successions are linked to climatic, oceanographic, and environmental variations [1] with the input of tectonic and/or diagenetic processes [2]. Several high-resolution works indicate that these sequences are related to orbital variations ([3] and references therein, [4]).

Deposition took place along a convergent margin within deformed basins, which recorded a progressive deterioration of environmental conditions at the onset of Messinian times [5–10]. Additionally, during Messinian and Plio-Pleistocene times, cyclic episodes of anoxia led to the deposition of organic-rich deposits (sapropels; [11,12]).

The sapropels (organic-rich layers) were likely deposited under conditions of minimum precession (maximum summer insolation), reflected in the Mediterranean basin by an increase in precipitation and runoff, which may have driven an increased stratification of surface waters. The marls are deposited during the subsequent rise in the precession index (reduction in summer insolation) and are reflected by a dry and cold climate, which corresponds to an increase in evaporation. This resulted in the mixing and reoxygenation of deep and bottom waters, reducing the preservation of organic matter [13–15]. Thus, it explains the low record of Total Organic Carbon (TOC), high content of Total Inorganic Carbon (TIC), and reducing conditions reflected by sulfur content >2% [7]. However, this lithological pattern is not consistent during the late Miocene along the whole Mediterranean: in the eastern part of the basin, sapropels are replaced by diatomites [4,16–21], while in the western side, the alternation of sapropel/marl and diatomite layers is dominant, like in the Sorbas section [11,22].

The present study focuses on the Torrente Vaccarizzo (TVCZ) Section from Sicily mainland. It shows exceptional metric-decimetric to millimetric lithological cyclicity highlighted by sapropel layers [23–25]. Detailed analysis on calcareous plankton, both foraminifers and nannofossils, important components of the pre-evaporitic successions, is useful for biostratigraphic and paleoceanographic/paleoenvironmental reconstructions [8,11,22,26–31].

However, a firm chronostratigraphic and biostratigraphic record of the Messinian pre-evaporitic interval in the Mediterranean may be hampered by the lack of chronostratigraphic data (i.e., magnetostratigraphic and radiometric dating) and/or the absence or scarceness of biostratigraphic markers due to the deterioration of the environmental conditions. Additionally, changes in the environmental conditions linked to local tectonics, river runoff, current circulation, and productivity may be peculiar to each sub-basin and therefore influence calcareous plankton assemblages. Therefore, biohorizons may retain a local significance.

The present study explores the use of abundance variation of calcareous plankton, recording an astrochronological cyclicity, to build an astrochronology-based age-model in the absence of other time constraints.

2. Geological Setting and Study Area

The study area is located in central Sicily (southern Italy) within the Caltanissetta Basin and is delimited by the villages of S. Caterina Villarmosa (west) and Villarosa (east). The Caltanissetta Basin [23,24,32,33] is made of a series of perched sub-basins (e.g., Corvillo, Pasquasia, etc.) developed on top of the orogenic Apenninic-Maghrebian Chain [34,35]. Here, the deformed substratum is made of Cretaceous-Oligocene Varicoloured Clays and Numidian Flysch quartz-arenites and clays (Figure 1). Thrust-top sedimentation started in the late Miocene with the deposition of deltaic silts, shallow-water fine sands, and prodelta marine clays of the Terravecchia Fm. The latter are usually shaped in badlands and at places overlaid by diatomaceous laminites of the Tripoli Fm. It consists of an alternation of clayey marls, laminated diatomites, and lime mudstones, forming the cyclic transitional deposits towards the onset of the Messinian Salinity Crisis (MSC). The succession, indeed, is followed by evaporitic deposits: gypsum, halite, and K- and Mg-salts, precipitated in the basin depocenters and passing laterally to carbonates, Calcare di Base Fm. (CdB) along the flanks of the basin margins [23,32–36]. The genesis of the CdB is either evaporitic or microbialitic/bacterial related [23,37–40]. Additionally, in the literature, the brecciated nature of the CdB is still a matter of debate. It has been interpreted as the product of in situ karstic/dissolution [23,32,33,36,39,41,42] and/or clastic re-sedimentation processes [38,43–46]. Despite the diverse facies, the CdB dominates the First Cycle of evaporites in outcrops [36] along with the gypsum, while thick halite layers and Mg- and K-salts are mainly preserved in the subsurface. There are several extractive salt mines among the districts of Agrigento, Caltanissetta, and Palermo (e.g., Petralia) within the Caltanissetta Basin. During the Messinian, an Erosional Surface (MES), linked with a drastic sea-level fall of the Mediterranean [36,38,43,47], separated the older First Cycle from the younger

Second Cycle evaporites ("Upper Evaporites" of [48]). The latter is made of gypsum, interbedded with detrital mud and gypse-arenites [33,36,49]. Evaporites are capped by the pelagic chalks and marls of Trubi Fm. in Pliocene time, testifying to the restoration of open marine conditions [50]. The succession passes upwards into an alternation of marls and calcarenites of the Enna Fm., marking the Plio-Pleistocene forced regression and the final emergence of the area [33,51–53].

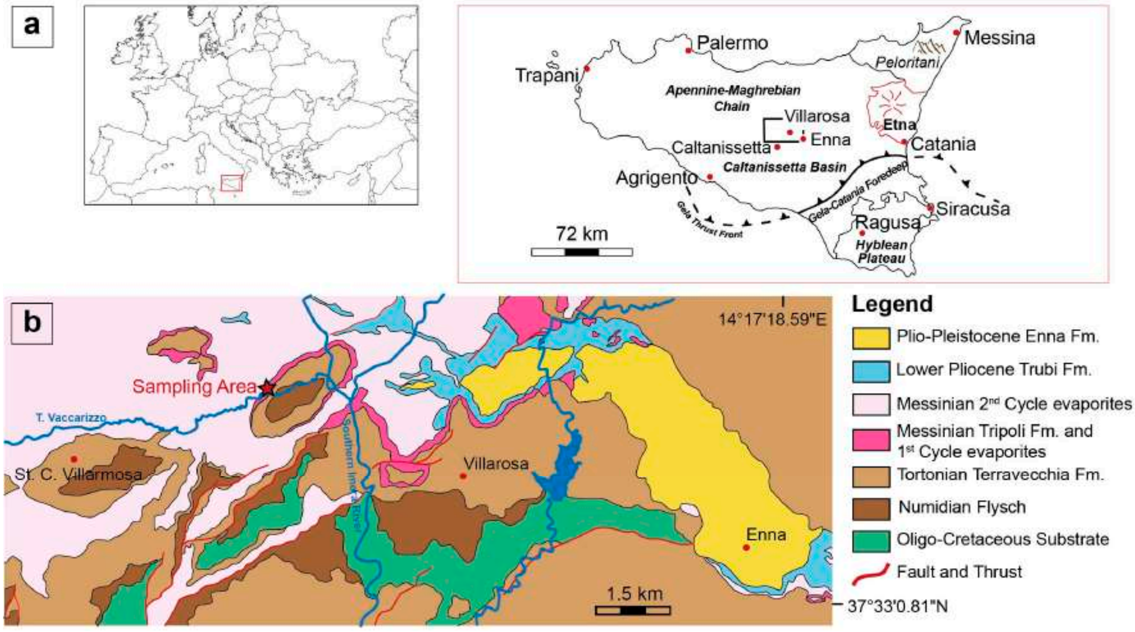

Figure 1. (**a**) Location of Sicily and main structural domains: Apenninic-Maghrebian Chain, Gela-Catania Foredeep, and Hyblean Foreland. (**b**) Simplified geological map of the central Sicily Caltanissetta Basin with section location (red star). After [7,36,54].

The overall sedimentary succession is highly affected by thrusts and folds, with thrust anticlines on the hanging wall (basin margins) and footwall synclines (deep basins). Here, we focus on the Tripoli Fm. cropping out along Torrente Vaccarizzo, close to Villarosa village (EN). The section is located on the northwestern limb of the Mucciarello anticline, plunging north-eastward.

3. The Stratigraphy of the TVCZ Section

According to the available literature, the thickness of the Tripoli Fm. varies from tens of meters, in the depocenter of some perched basins (e.g., Gaspa, Pasquasia), to almost zero, in the marginal high-standing areas (e.g., Sambuco). Four are the main lithologies that generally alternate within the Tripoli succession [23]: (i) clays and marls; (ii) carbonaceous beds; (iii) diatomaceous laminites; (iv) lime mudstones.

The study area lies along the southern bank of the Vaccarizzo Stream. Here, a 27-meter-thick measured section of Tripoli Fm. crops out, and it is overlain by more than 30 meters of CdB beds. The strata show an average strike and dip of N 215°/50° along the northwestern flank of the Mucciarello Anticline [36], which plunges north-eastward.

The developed stratigraphic log (Figure 2) can be divided into four different sectors:

(i) In the first 6.5 m, dark grey to grey silts are dominant and related to the topmost part of the Terravecchia Fm. Their maximum thickness is about 2 m. In particular, the bottom part (0–4 m) is characterized by the alternation of black clays (sapropels), silts, and marls, which gradually pass upwards into silts. The latter are followed by a 25 cm layer of lime mudstone.

(ii) From 8 to 19 m, the succession is dominated by the alternation of sapropels and marls. From 13 m upwards, three layers of laminated diatomites, of about 30 cm each, precede the deposition of a 20 cm thick gypsum bed that marks the first evaporitic bed of the section. On top of it, the succession shows a 1.4 m thick sapropel overlain by 60 cm of marls.

(iii) From 19 m to 27 m, laminites and marls of different thicknesses are alternated. Specifically, the lower part (19–22 m) is dominated by a highly slumped dark grey laminite (over 1 m thick) with interbedded gypsum layers. A 20 cm black level interrupts the facies alternation of laminites and marls.

(iv) From 27 m to the top, tens of meters thickness of CdB beds follow. They are alternated with thin layers of marls and sapropels. Overall, marls show a grey to dark grey color, which becomes greenish towards the CdB beds.

Figure 2. TVCZ Section. (**A**) View from south of the outcrop. It is possible to note the cyclic alternation of white and black lithologies getting younger eastward. (**B**) Simplified log of the section projected on the interpreted outcrop picture.

The section shows several black, organic-rich intervals that have been the object of a previous study and revealed a change from oxic/dysoxic to dysoxic/anoxic conditions towards the younger part of the section characterized by specific biomarkers (i.e., squalene produced by marine hypersaline organisms [7]). Previous works have already pointed out a connection between lithological and astronomical cycles [5,6,23,25,33,55,56]. Therefore, this section seems to be promising to explore also the biological events preceding the onset of the MSC in response to climatic/environmental changes.

4. Materials and Methods

4.1. Sampling Strategy

A total of 69 samples within the 29.4 m succession have been sampled during different field-work campaigns. For this reason, the original denomination of samples was renamed according to Table S1 in Supplementary Materials.

Sampling spacing varies between 20 and 50 cm and integrates a previously scattered sampling aimed at organic geochemistry analysis made by [7]. Two samples (960 cm and 2250 cm) for paleomagnetic analysis have also been collected. A first screening permitted the distinguishment of barren samples from oligotypical to diversified assemblages, as reported in Table S1 in Supplementary Materials.

4.2. Quantitative Analysis: Calcareous Nannofossils

For the study of calcareous nannofossils, a total of 69 smear slides, prepared according to standard methodology (e.g., [57]), were analyzed using a polarizing light microscope at 1000× magnification. A total of at least 300 specimens larger than 3 μm were counted in random fields of view. Specimens < 3 μm in size were not considered.

For species with low abundances, we extended the counting to 1 mm^2 of the slide, corresponding to about 100 fields of view. The frequency of *Discoaster* and *Helicosphaera* species was calculated within at least 30 specimens belonging to the *Discoaster* and *Helicosphaera* genera.

Results are thus presented as (i) percentages within the total assemblage; (ii) percentages within the *Discoaster* and *Helicosphaera* genera; (iii) the number of specimens per mm^2.

Nannofossils in the studied samples show preservation from moderate to good. Occasional overgrowths are present on some specimens of the *Discoaster* genus, but this feature never prevents their identification at the species level. Reworking may be significant on some levels. Few samples (TVCZ 24, 36, 42, and 46) yield scarce or oligotypical nannofossil assemblages. Barren samples are listed in Table S1 (Supplementary Materials).

For this study, we adopted the calcareous nannofossil biostratigraphic scheme for the Mediterranean area of Di Stefano et al. [58].

4.3. Quantitative Analysis: Planktonic Foraminifers

For the analysis of the planktonic foraminifers, 63 samples along the whole section (Table S1 in Supplementary Materials) were firstly dried and weighted and then washed through a 63 μm sieve. However, only the fraction greater than 125 μm was considered for quantitative analysis. From this, about 300 specimens of planktonic foraminifers were picked and counted in sample splits. The quantitative distribution pattern of selected planktonic foraminifers categories, having biostratigraphic and/or paleoclimatic significance, has been recorded. The planktonic foraminifer biostratigraphic scheme, the range chart, and the chronology of planktonic foraminifer biohorizons, adopted in the present work, are from [59].

Planktonic species were grouped into the following categories: (1) neogloboquadrinids: including *Neogloboquadrina acostaensis* (Blow) and *N. humerosa* (Takaianagi and Saito); (2) *Orbulina* spp.; (3) *Turborotalita multiloba* (Romeo); (4) *Turborotalita quinqueloba* (Natland); (5) *Globorotalia scitula* (Brady); (6) globigerinids: including *Globigerina* spp. and *Globigerinoides* spp.; (7) *Globigerinita* spp.: including G. *glutinata* (Egger), and *G. uvula* (Ehrenberg). Raw data of microfossils were transformed into percentages over the total abundance. The counted specimens of *N. acostaensis* have been separated on the basis of their coiling direction and plotted as ratios of dx/and sx/total number of *N. acostaensis.*

5. Calcareous Plankton Biostratigraphy Preceding MSC

The pre-evaporitic interval has been widely studied from the western to central and eastern Mediterranean, ranging from Spain through Apennines, Sicily, and Greece [5,6,27,38,60–68]. Thus, a biostratigraphic scheme based on calcareous plankton bioevents is well-established so far for the Messinian time in the Mediterranean area. It has been calibrated by integrating classical quantitative biostratigraphy with magnetostratigraphy and cyclostratigraphy, giving rise to a detailed bio-chronological framework of the interval preceding the MSC (Table 1).

Table 1. Messinian biostratigraphic horizons from Mediterranean sections and inferred ages according to the available literature. (*) = Tie point used for the age-model. FCO = First Common Occurrence; FAI = First Abundance Influx.

		Present Study	**Other Mediterranean Sections**									
	Bioevents	**Sample**	**Sorbas Basin**	**Falconara/ Gibliscemi**	**Fanantello**	**Trave**	**M. dei Corvi**	**M. del Casino**	**Metochia**	**Pissouri**	**Piedmont Basin**	**Kalamaki (Ionian Sea)**
E.(*)	*Sphenolithus* + *Helicophaera* peak I = “MSC onset event”	TVCZ-49	(*)5.99 [68]		5.97 [63]					5.99 [64]	5.98 [66,67]	
D.	Last influx *T. multiloba*	TVCZ-36	6.07 [11,59]	6.07 [17,18,59]								
C.	*N. acostaensis* sx/dx coil. change	TVCZ-17	6.36 [11]	6.337 [5] 6.35 [6] 6.34 [56]						6.342 [64]		
	Neogloboquadrinids sx/dx coil. change						6.37 [69]					
	FCO *N. acostaensis* dx			6.44 [17,18]								
B.	Influx *H. selli*	TVCZ-14				6.49 [27]						
	FCO *H. selli*					6.50 [65]		6.96 [63]		6.53 [64]		
	FCO cf. *H. selli*								6.48 [62]			
A.(*)	“FAI *T. multiloba*”	TVCZ-14	(*)6.412 [11]									
	FCO *T. multiloba*			6.40 [6] 6.41 [17,18] 6.415 [56]					6.415 [70]			6.415 [31]

However, the already documented evolution of the calcareous plankton towards low diversity and oligotypic assemblages until their complete disappearance is still of great interest.

In Sicily, noteworthy successions documenting the conditions preceding the MSC are represented by the Falconara, Gibliscemi, Capodarso, Serra Pirciata, and Marianopoli Sections (Reference on Table 1). Reference sections fall within foraminifers Biozones MMi 13c and MMi 13d of [59] and nannofossil Biozone MNM11d of Di Stefano et al. [58].

Selected calcareous plankton bioevents have been recorded in the TVCZ Section as well and are discussed in detail in the following sections.

5.1. Calcareous Nannofossils in the TVCZ Section

The results of the quantitative analysis of calcareous nannofossils in the TVCZ Section are shown in Figure 3, which illustrates the frequencies of the main components within the total assemblage (average percentages > 1%, Supplementary Materials Tables S2 and S3) and in Figure 4, where the frequencies of ceratoliths and discoasters are presented.

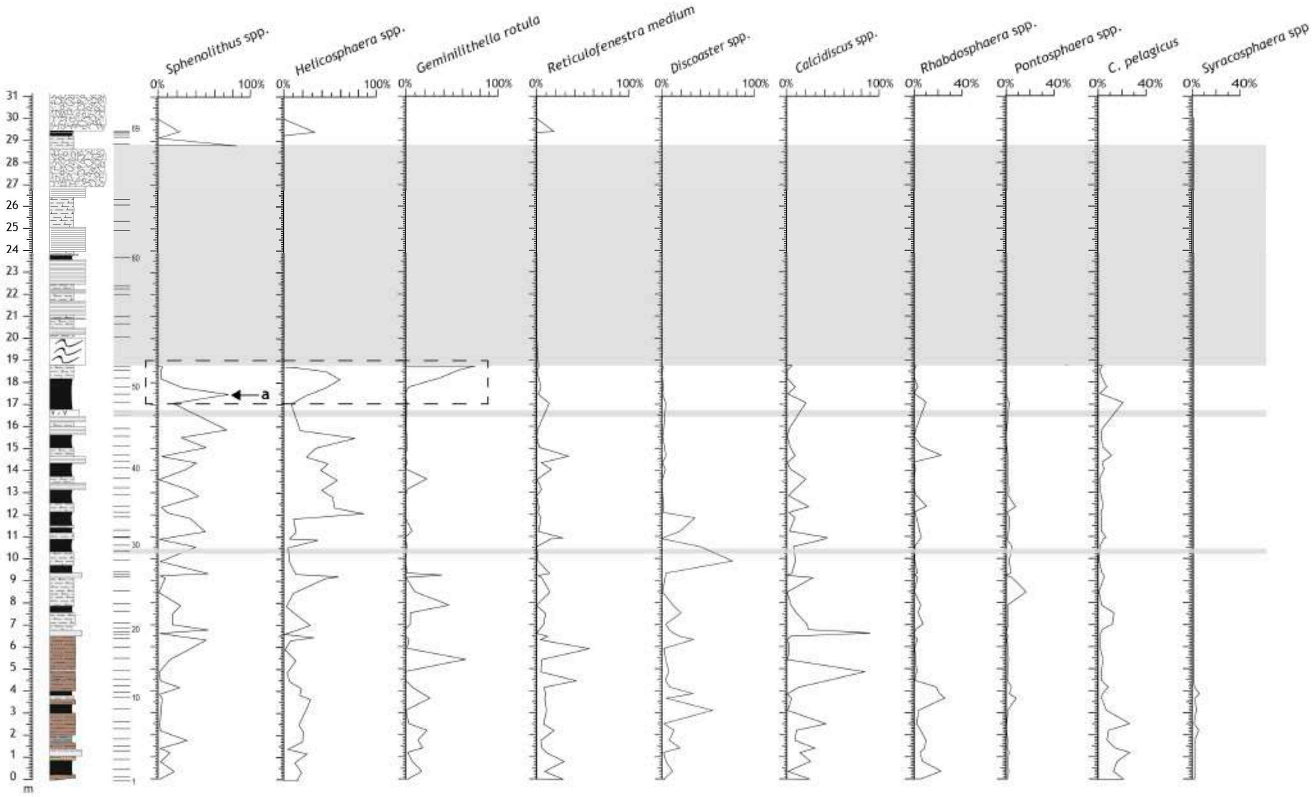

Figure 3. Quantitative distribution patterns of main taxa of the nannofossil assemblages (>1%) (counting method described in Section 4.2). The grey areas indicate the intervals of barren samples. The dashed rectangle indicates the "MSC onset event" described in the text. (a) abundance peak of *Sphenolithus* spp.

Reticulofenestra medium-sized (3–7 µm) is the most abundant taxon, representing, in some cases, over 50% of the total assemblage (Figure 3). This category also includes *Reticulofenestra rotaria,* which was recorded in few samples with very low frequencies. Other relevant components are the helicoliths, mainly represented by *Helicosphaera carteri* and by *H. sellii,* which show a discontinuous sporadic presence and an abundance peak in the lower part of the section ("a" in Figure 3). *Sphenolithus* spp. (*S. abies* + *S. neoabies*), well represented along the whole section, shows a remarkable rhythmic pattern as well as the *Calcidiscus* genus (*C. leptoporus* + *C. macintyrei*) (Figure 3).

Similar behavior is shown by *Geminilithella rotula* and *Rhabdosphaera* spp. (mainly represented by *R. clavigera;* Figure 3); *Pontosphaera* spp. is present in the central part of the succession with maximum frequencies of 20%, and *Syracosphaera* spp. in the lowermost part with frequencies lower than 10% (Figure 3).

Coccolithus pelagicus is present along the section and shows a fluctuating trend, generally with low abundance (Figure 3).

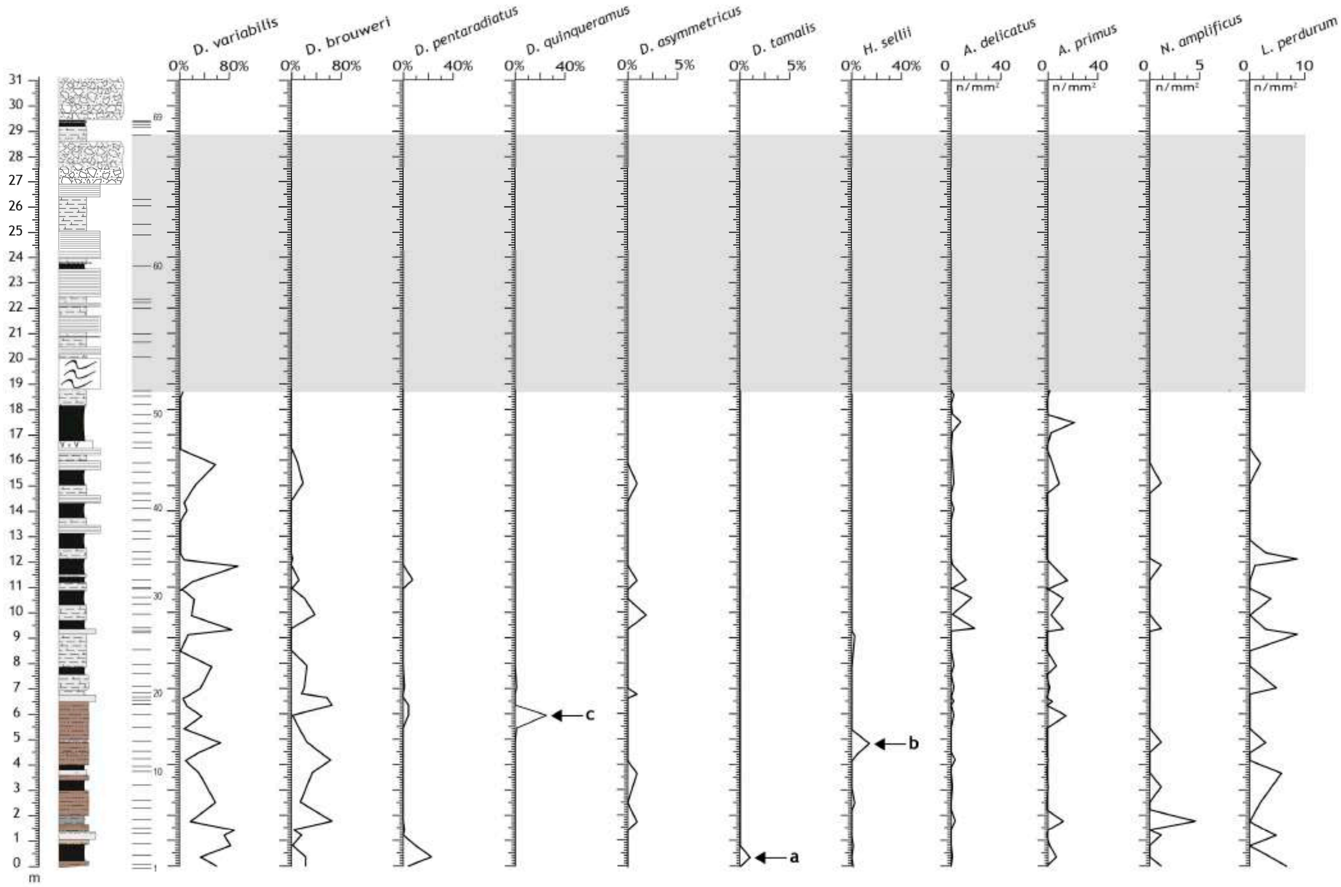

Figure 4. Quantitative and semiquantitative distribution patterns of *Discoaster* and ceratholiths, according to the counting methods described within Section 4.2. The grey area indicates the interval of barren samples. Arrows with letters indicate bioevents discussed in the text (a = *D. tamalis* Influx; b = *H. sellii* Influx; c = *D. quinqueramus* Influx).

Discoaster specimens are common in the lower part of the succession and almost absent from 12 m upward. Their distribution pattern is characterized by wide and rapid fluctuations ranging from very high percentages (in the central part of the section) to zero. Within the *Discoaster* genus, *D. variabilis* and *D. brouweri* are the most common. *Discoaster pentaradiatus* and *D. asymmetricus* are discontinuously present in low percentages. *Discoaster quinqueramus* and *D. tamalis* depict two peaks in the basal part of the section (Figure 4).

Ceratholiths are important components of the nannofossil assemblages in the Messinian time interval. In the TVCZ Section, they are represented by *Amaurolithus primus*, *A. delicatus*, and *Nickilithus amplificus*. These taxa are present from the base of the section and are characterized by a fluctuating trend.

The remarkably highly fluctuating presence of *Lithostromation perdurum* is noteworthy and already documented within an equivalent stratigraphic interval in the Sorbas Basin [12].

According to our results, the TVCZ section should be younger than the first occurrence of *Nicklithus amplificus* (thus falling within Zone MNN11c of Di Stefano et al. [58]), which is considered a sufficiently reliable event in the Messinian, with an attributed age of 6.69 My [62].

Helicosphaera carteri has been a main component of the helicoliths assemblages since the Early Miocene—e.g., [58,71,72]. On the contrary, the presence of *Helicosphaera sellii* is traditionally assigned to the early Pliocene. Nevertheless, the sporadic occurrence of this species in the Messinian is well documented in several Mediterranean sections—e.g., [27,62,65,73]. In the TVCZ section, the *H. sellii* abundance peak detected at about 5 m (sample TVCZ-14; "a" in Figure 3) is well comparable with the *H. sellii* influx described by Iaccarino et al. [65] with an attributed age of 6.50 My.

In the uppermost part of the section, an abundance peak of *Sphenolithus* spp. ("a" within the dashed rectangle in Figure 3) is slightly followed by *G. rotula* and *H. carteri* spikes. This precise sequence of abundance peaks was previously reported in different Messinian sections ("MSC onset bioevent") [29,68]. The ages attributed to the base of this event are reported in Table 1.

The presence of *Discoaster quinqueramus* in Mediterranean sections was widely debated—e.g., [62]. Nevertheless, our findings testify that "true" *D. quinqueramus* occurs in the TVCZ Section as previously documented—e.g., [27,65,74]. In the specific, an abundance spike of the species is observable within sample TCVZ-16 ("c" in Figure 4). *Discoaster tamalis* has been a significant component of *Discoaster* assemblages since the late Zanclean. Nevertheless, the sporadic presence of the species is also documented in some Mediterranean sections since the Messinian time interval—e.g., [27,65]. Yet, the presence of *D. tamalis* in the lowermost part of the section (sample TVCZ-2; "a" in Figure 4) is not comparable with the similar event described by Iaccarino et al. [65] and Di Stefano et al. [27] ("*D. tamalis* Influx") occurring below the first occurrence of *N. amplificus* and dated 6.9–6.79 My [65].

The interval between samples TVCZ-54 and TVCZ-64 does not contain calcareous nannofossils. Yet, few samples (TVCZ-65, TVCZ-69) from the clay horizons between CdB strata yield scarce, oligotypic assemblages mainly composed of specimens from the *Sphenolithus* and *Helicosphaera* genera.

5.2. Planktonic Foraminifers in the TVCZ Section

The preservation of the planktonic foraminifers assemblages is variable in the TVCZ Section. From the bottom of the section up to 320 cm, within the silts and marly silts, the plankton community is abundant and moderately to well preserved (Supplementary Materials Table S4). From 320 cm up to 1555 cm, within silts and grey-black shales, diatomitic laminites, and lime mudstones, preservation becomes moderate to poor, and planktonic association is generally common. The distribution of planktonic foraminifers is almost continuous up to 1650 cm, except for three barren intervals in the lower-middle part of the section, located respectively from bottom to top, at 685 cm, 1290–1365 cm, and 1470 cm. From 1650 cm upward, the samples are barren of planktonic foraminifers but contain only a few species of benthic foraminifers, such as *Bulimina echinata*, *B. aculeata*, *Bolivina dilatata*, and *Uvigerina* spp.

The results of the quantitative analysis of plankton foraminifers in the TVCZ Section are shown in Figure 5, where the frequencies of the main taxa within the total assemblage (average percentages > 1%) are plotted. Additionally, the main biohorizons with biostratigraphic significance are here presented, discussed, and compared with previous findings.

From the base of the section to about 450 cm, the planktonic association is quite diversified, made of abundant globigerinids (*Globigerinoides obliquus* and *G. quadrilobatus* group, *Globigerina* spp.), *Orbulina* spp., mainly sinistral coiling *Neogloboquadrina acostaensis*, followed in abundance by *Neogloboquadrina* spp. (mainly *N. humerosa)* and *Globigerinita* spp. (Figure 5). Rare specimens of the *Globorotalia scitula* group have also been recorded.

A remarkable event present in the TVCZ Section is the First Abundance Influx (FAI) of *T. multiloba,* renamed after Sierro et al. ("First Abundant influx" *T. multiloba*, [11]) in sample TVCZ-14 at 495 cm (Table 1), with a percentage of 14.7% (A in Figure 5). *T. multiloba* is an endemic form of the Mediterranean and has been considered an ecophenotypic variant of *T. quinqueloba*. The bioevent (named "First Abundant Influx" or "First Common Occurrence by different authors, e.g., Table 1) has been widely used for biostratigraphic correlations in the Mediterranean. It characterizes subzone MMi 13c [5,11,31,59,70] and is dated at 6.4 My (Table 1) at Falconara Section (Sicily), Sorbas and Abad sections (Spain), and Kalamaki (Ionian Sea) and Metochia (Gavdos Island, Greece). Bellanca et al. [6] and Blanc Valleron et al. [56] reported the second and last influxes at the Falconara section, respectively, dated at 6.28 My and 6.07 My.

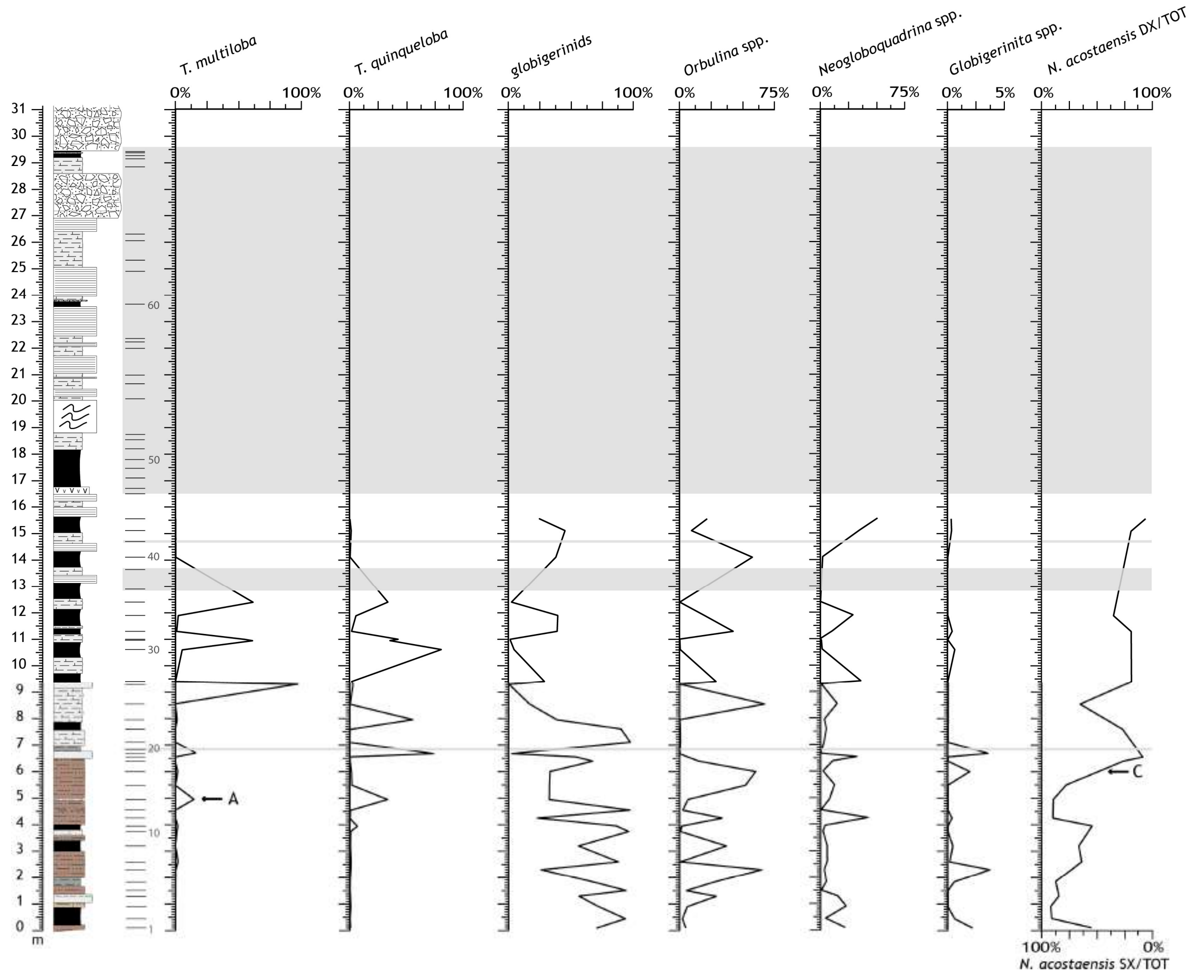

Figure 5. Quantitative distribution patterns of main groups/taxa of the planktonic foraminifers assemblages, grouped as described in the methodology section. The grey area indicates barren samples. (A) First Abundance Influx (FAI) of *T. multiloba*; (C) sx/dx coiling change in *N. acostaensis*.

Another remarkable biohorizon is the change from sinistral to dextral coiling of *N. acostaensis.* The event is identified by the dominance of dextral coiling *N. acostaensis* over the total of *N. acostaensis* (percentage greater than 50%). *N. acostaensis* sx/dx coiling change (C in Figure 5) is recorded between TVCZ-15 (550 cm) and TVCZ-17 (640 cm) since the latter bears a low number of specimens. The event has been reported in the literature from different sections with ages ranging from 6.337 to 6.36 My. Authors [17,18] describe a FCO of dextral *N. acostaensis* dated at 6.44 My from the Falconara/Gibliscemi Section.

Several additional influxes of *T. multiloba* have been recorded in the TVCZ Section in samples TVCZ-19 (16.19%), TVCZ-26 (97.04%), TVCZ-31 (61.40%), and TVCZ-36 (61.80%), respectively, at 670, 930, 1095, 1240 cm. The taxon occurs in poorly diversified and oligotypic associations together with *T. quinqueloba* (Table 1). This points to stressed environmental conditions preceding the Messinian Salinity Crisis [59].

An influx of sinistral *N. acostaensis* is recorded at TVCZ between samples TVCZ-24 (855 cm) and TVCZ-23 (795 cm).

In the TVCZ Section, up to 9 peaks in abundance of *Orbulina* spp. have been recorded and will be described and commented in the next paragraph. Relative abundance fluctuations of *Orbulina* spp. and high peaks (80–90% “orbulinites” event, [59]) have been previously recorded in pre-evaporitic deposits.

The disappearance of planktonic foraminifers preceding the onset of the MSC is reported in correspondence with a first gypsum layer (1650 cm, Figure 5) within sample TVCZ-46. This event is still a matter of debate and is considered either diachronous or synchronous throughout the Mediterranean and will be discussed in the next paragraph [6,11,17,18,38,56,75–77].

6. Age-Models

A chronostratigraphic frame of the events preceding the MSC in the TVCZ Section was first attempted through biostratigraphic data. Unluckily, the test on paleomagnetic properties revealed the absence of natural remanent magnetization (NRM) in the sampled intervals. For such reason, two bioevents, considered synchronous and widespread in the Mediterranean (Table 2), have been then selected as Tie Points (TPs):

(1). The First abundance influx (FAI) of *T. multiloba* in Sample TVCZ-14 (495 cm from the base) and dated at 6.412 My, according to Sierro et al. [11], also described as "FCO of *T. multiloba*" and dated at 6.40 My [6], 6.41 My [17,18], and 6.415 My [56]. Therefore, an age of 6.42 My [5,11,17,18,56] has been fixed as TP for the preliminary age-model.

(2). *Sphenolithus* + *Helicosphaera* peak I coincident with the base of the "MSC onset event" ("a" within the dashed rectangle in Figure 3) in sample TVCZ-49 (1750 cm from the base), dated at 5.99 My by Mancini et al. [68].

In the absence of further fixed TPs, the resulting age-model (Figure 6) is presented by a straight line that defines a homogeneous sedimentation rate of 2.92 cm/ky along the considered tract of the section. This age-model does not prove to be entirely reliable, considering the lithological variations affecting the examined section. However, it allows the assignment of numerical ages to the other bioevents in between (Figure 6). Their ages are comparable with the ones reported in the literature.

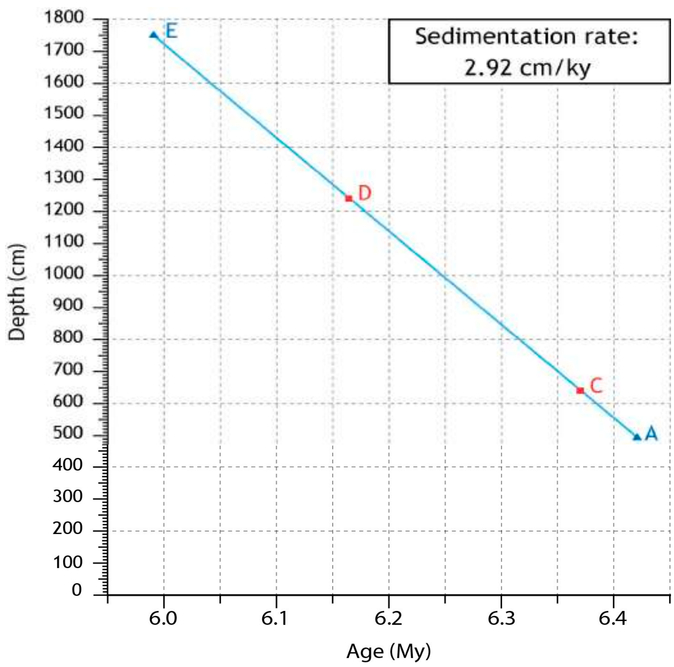

Figure 6. Preliminary age-model of the TVCZ Section based on two biostratigraphic TPs (in blue): (A) *T. multiloba* FAI (in sample TVCZ-14) and (E) *Sphenolithus* + *Helicosphaera* peak I (=base of the "MSC onset event" in sample TVCZ-49). Derived ages of the bioevents (C) (*N. acostaensis* sx/dx coiling change) and (D) (Last influx *T. multiloba*).

Yet, the depth-age graph of Figure 6 may be used as an initial chronological framework to retrieve the Milankovitch cyclicity that could derive from the distribution pattern displayed in the TVCZ Section by *Orbulina* spp. (Figure 5), which seems to provide a better response than other taxa.

In fact, *Orbulina* thrives in relatively warm and oligotrophic surface waters [78,79], and is tolerant to high salinity conditions [80–82]. According to the existing literature, *Orbulina* is dominant in Mediterranean Messinian successions, thus, representing a good proxy in stressed environments [1,17,18,56,83–85]. Furthermore, it seems to fit well with Milankovitch cyclicity—e.g., [21,22,28]. In the specific, *Orbulina* seems to display a similar pattern recorded by the genus *Globigerinoides*, which shows an in-phase correlation with the Eccentricity curve: *Globigerinoides* maxima—carbonate minima, Eccentricity maxima [28] as also reported from several Pliocene successions of Sicily [86]. In this paper, *Globigerinoides* spp. and *Globigerina* spp. have been grouped and counted within globigerinids (Figure 5). We focused instead on *Orbulina* spp. variation abundance, since several Authors [18,59] report from the Mediterranean area, starting from 6.40 My, the well-known "orbulinites" event characterized by 80–90% of *Orbulina* spp.

For spectral analysis, the *Orbulina* spp. original data from the TVCZ Section were linearly interpolated through the software Past 4.11 [87] and equally spaced at intervals of 10 ky (Figure 7a), according to the preliminary age-model (Figure 6). The autocorrelation test on the *Orbulina* spp. curve (Figure 7b) proves that it contains a periodicity after 10 points (~100 ky) that corresponds to a frequency of 0.0957 cycles/10 ky (Figure 7c). This frequency is very similar to the high-frequency Eccentricity for the considered time interval, which is 0.1035 cycles/10 ky (La2004 solution by Laskar et al. [88], available on the IMCCE website—https://www.imcce.fr/ (accessed on 24 March 2023)). Moreover, the cross-correlation test (Figure 7d) between the *Orbulina* spp. and the Eccentricity shows a phase relationship between the two curves.

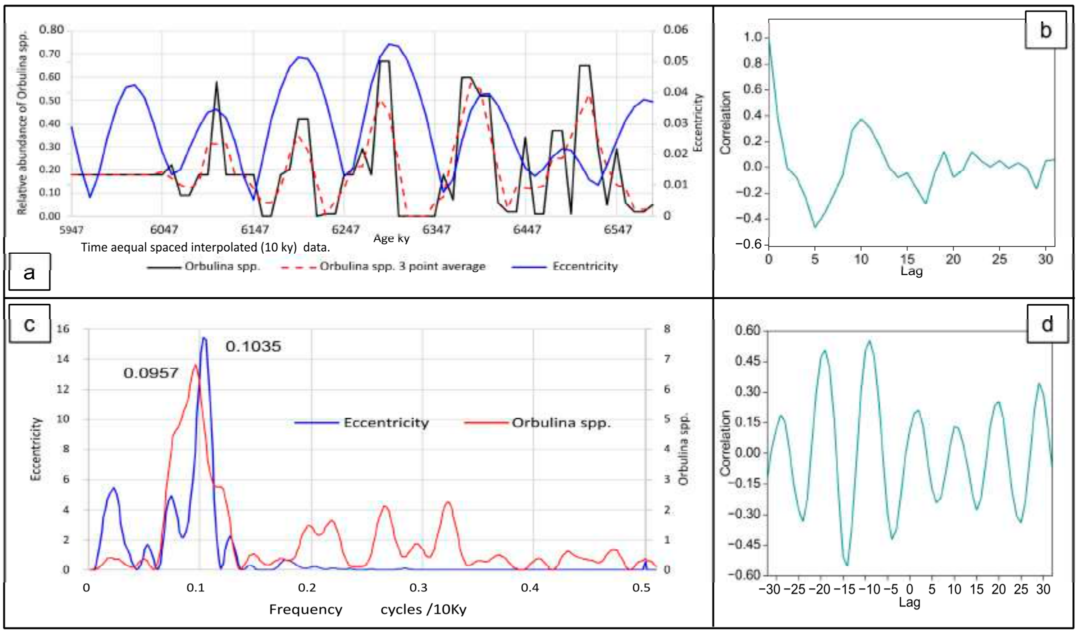

Figure 7. Signal analysis of the *Orbulina* spp. distribution pattern in the TVCZ Section according to the preliminary age-model illustrated in Figure 6. *Orbulina* spp. abundance has been plotted vs. time and interpolated with a constant spacing of 10 ky. (**a**) Comparison between Eccentricity and *Orbulina* spp. curves, showing that the main peaks almost coincide. (**b**) Autocorrelation test of *Orbulina* spp. with a main peak at lag 10 (period of ~100 ky). (**c**) Power spectrum of *Orbulina* spp. and Eccentricity with two peaks with maximum power and frequency of ~0.1 cycles/10 ky; (**d**) Cross-correlation test between *Orbulina* spp. and Eccentricity; at lag 0, the two curves are in phase and remain in phase every 10 points (~100 ky).

Five peaks with a frequency of ~0.1 cycles/10 ky are confidentially recognized within the *Orbulina* spp. distribution pattern (Figure 8a). Thus, the ages of these *Orbulina* peaks (Table 2) correspond to the Eccentricity maxima in the ~100 ky period (Figure 8b). These can be used as TPs for the construction of the age-model illustrated in Figure 8c. Based on this age-model, the ages of all sampled points may be re-calculated (Table 2).

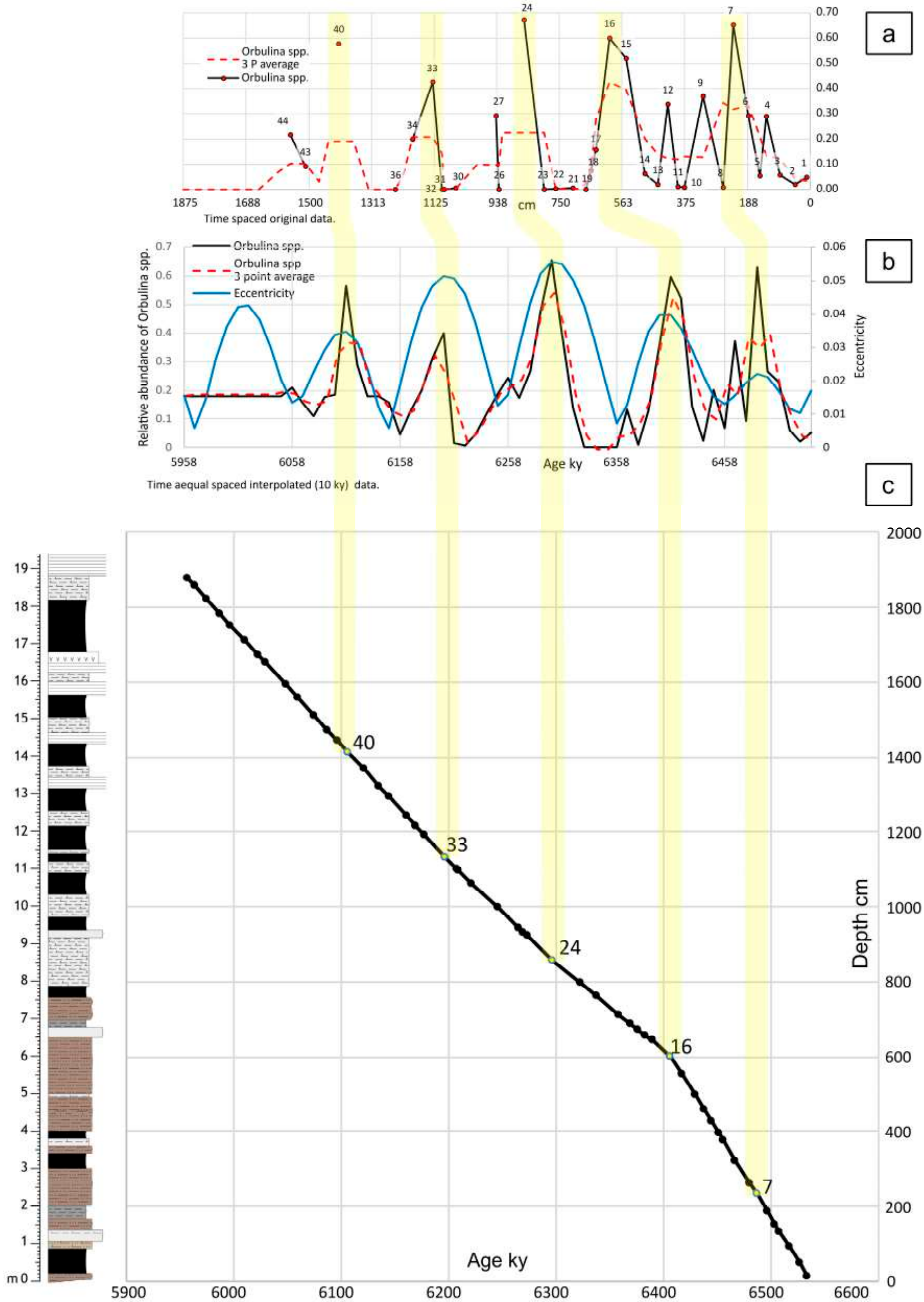

Figure 8. (**a**) Abundance variation curve of *Orbulina* spp. vs. depth. (**b**) Abundance variation curve of *Orbulina* spp. vs. time. (**c**) Age-model for the TVCZ Section based on astrochronology, where maximum amplitude peaks of *Orbulina* spp. were correlated with maximum amplitude peaks of Eccentricity. Data are interpolated and spaced with a step of 10 ky. The yellow bands correlate with the *Orbulina* spp. curve vs. depth and the *Orbulina* spp. and Eccentricity curve vs. time.

Table 2. Derived ages for each sampled point in the TVCZ Section, according to the age-model of Figure 8c. The yellow labels correspond to the ages of the samples where the *Orbulina* spp. maxima (used as TPs) occur.

New Sample Numeration	Original Sample Numeration	Position (cm)	Sedim. Rate (cm/ky)	Age (ky)	New Sample Numeration	Original Sample Numeration	Position (cm)	Sedim. Rate (cm/ky)	Age (ky)
TVCZ 53	22	1875	3.11	5957.74	TVCZ 26	45	930	2.75	6269.93
TVCZ 52	25	1855		5964.16	TVCZ 25	6B	920		6273.56
TVCZ 51	24	1820		5975.41	TVCZ 24	6	855	2.32	6297.20
TVCZ 50	21	1780		5988.27	TVCZ 23	5	795		6323.08
TVCZ 49	23	1750		5997.91	TVCZ 22	4	760		6338.18
TVCZ 48	20	1710		6010.77	TVCZ 21	3	710		6359.75
TVCZ 47	19 bis	1670		6023.63	TVCZ 20	2	685		6370.53
TVCZ 46	19	1650		6030.06	TVCZ 19	43	670		6377.00
TVCZ 45	18B	1590		6049.34	TVCZ 18	1	655		6383.47
TVCZ 44	18 bis	1555		6060.59	TVCZ 17	42	640		6389.95
TVCZ 43	18	1510		6075.06	TVCZ 16	46	600	4.63	6407.20
TVCZ 42	17	1470		6087.91	TVCZ 15	47	550		6418.01
TVCZ 41	16B	1440		6097.56	TVCZ 14	48	495		6429.90
TVCZ 40	16	1410		6107.20	TVCZ 13	49	455		6438.55
TVCZ 39	15	1365		6121.66	TVCZ 12	50	425		6445.04
TVCZ 38	14B	1320		6136.13	TVCZ 11	51	395		6451.52
TVCZ 37	14	1290		6145.77	TVCZ 10	52	375		6455.85
TVCZ 36	13	1240		6161.84	TVCZ 9	53	320		6467.74
TVCZ 35	12B	1215		6169.88	TVCZ 8	54	260		6480.71
TVCZ 34	12	1190		6177.91	TVCZ 7	55	230		6487.20
TVCZ 33	11	1130	2.75	6197.20	TVCZ 6	56	185		6496.93
TVCZ 32	10	1100		6208.11	TVCZ 5	57	150		6504.50
TVCZ 31	44	1095		6209.93	TVCZ 4	58	130		6508.82
TVCZ 30	9	1060		6222.65	TVCZ 3	59	90		6517.47
TVCZ 28	7B	995		6246.29	TVCZ 2	60	45		6527.20
TVCZ 27	7	940		6266.29	TVCZ 1	61	10		6534.77

According to the new age-model, the spectral analysis was performed again on the *Orbulina* spp. distribution pattern in the TVCZ Section, obtaining the results illustrated in Figure 9 that can be compared with the one in Figure 7. The autocorrelation test of *Orbulina* spp. (Figure 9a) is much clearer and linear than the previous one (Figure 7b), showing a repetitiveness every 10 points. The simple periodogram of *Orbulina* spp. (Figure 9b) shows a frequency peak at 0.1035 cycles/10 ky that is well aligned with that of Eccentricity, while the two peaks were slightly misaligned according to the preliminary age-model (Figure 7c). In addition, the cross-correlation test between *Orbulina* spp. and Eccentricity still shows a good phase relationship between the two curves (Figure 9b).

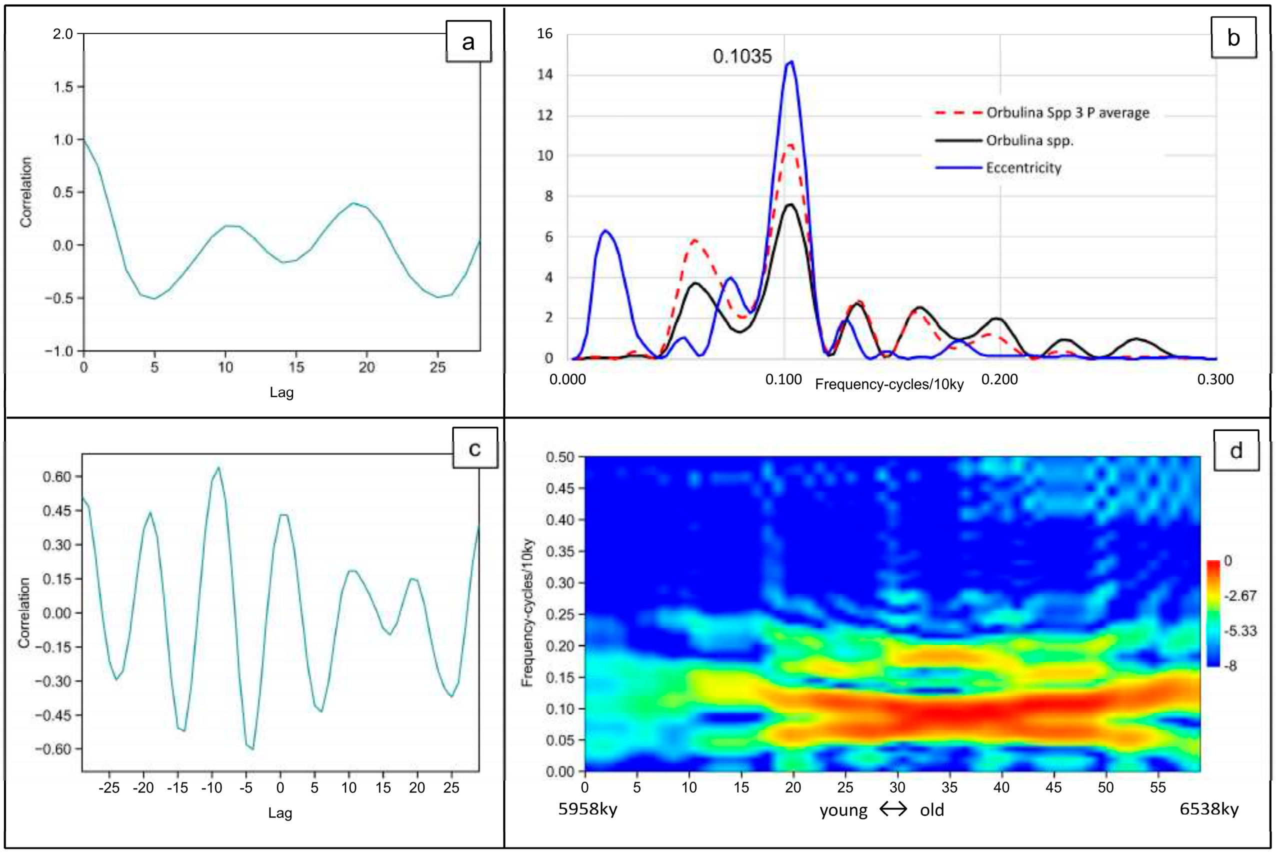

Figure 9. Signal analysis of *Orbulina* spp. distribution pattern in the TVCZ Section according to the age-model of Figure 8c. (**a**) Autocorrelation test of *Orbulina* spp. clearly showing 10-lag periodicities (~100 ky); the signal is clearer than in the autocorrelation test of Figure 7b, where time conversion derived from the preliminary age-model of Figure 6; (**b**) Cross-correlation test between *Orbulina* spp. and Eccentricity curves, which shows a 10 points phase relation between the two curves; (**c**) Simple periodogram of *Orbulina* spp. distribution pattern compared to the Eccentricity one, showing that their maximum power peaks are aligned; (**d**) Evolutive harmonic analysis of *Orbulina* spp. The high-power frequency is lacking in the youngest part of the studied succession, where foraminifers are absent.

Finally, the evolutive harmonic analysis (short-time Fourier Transform in Past 4.11) on *Orbulina* spp. (Figure 9d) shows the already recognized significant frequency of ~0.1 cycles/10 ky but also indicates that this signal is not homogeneous along the section. This frequency is not well visible along the youngest part of the succession since *Orbulina* spp. is absent.

According to the inferred age of the considered interval (6.536–5.958 My), the low-frequency Eccentricity signal of about 0.025 cycles/10 ky (periodicity of ~400 ky) is difficult to detect, considering that the section interval deposited in 580 ky, thus recording only almost 1.5 cycles.

7. Discussion

The astrochronological age-model (Figure 8c; Table 3) clearly shows the variation in the sedimentation rate along the succession. As expected from field observations, it is higher in the lower part (4.63 cm/ky), where terrigenous lithologies of the Terravecchia Fm. crop out, and much lower in the upper part (from 2.32 to 3.11 cm/ky) where diatomitic laminites and marls, assigned to the Tripoli Fm., occur.

Table 3. Bioevents and calculated ages from preliminary and astrochronological age-models. * Ages calculated according to the preliminary age-model (Figure 6). ** Ages calculated according to the astrochronological age-model (Figure 8c and Table 2).

Sample (cm)	Events in the TVCZ Section	Age * (My)	Age ** (My)
TVCZ-53 (1875)	MSC onset	—	5.957
TVCZ-53 (1875)	Top CN_MSC_OE	—	5.957
TVCZ-49 (1750)	Base CN_MSC_OE	5.99 (TP)	5.997
TVCZ-46 (1650)	Disappearance of planktonic foraminifers	6.024	6.030
TVCZ-36 (1240)	Last local influx *T. multiloba*	6.165	6.161
TVCZ-31 (1095)	IV local Influx *T. multiloba*	6.214	6.209
TVCZ-26 (930)	III local Influx *T. multiloba*	6.271	6.269
TVCZ-24 (855)	local Influx sx *N. acostaensis*	6.297	6.297
TVCZ-19 (670)	II local Influx *T. multiloba*	6.360	6.377
TVCZ-17 (640)	sx/dx coiling *N. acostaensis*	6.370	6.389
TVCZ-16 (600)	Influx *D. quinqueramus*	6.384	6.407
TVCZ-14 (495)	FAI *T. multiloba*	6.41 (TP)	6.429
TVCZ-14 (495)	Influx *H. selli*	6.420	6.429
TVCZ-2 (45)	II Influx *D. tamalis*	6.574	6.527

In addition, it is now possible to assign ages to the calcareous plankton events detected along the section (Table 3) and to compare them with the same or similar events described in other Mediterranean sections.

7.1. Age of Calcareous Nannofossils Bioevents in the TVCZ Section

According to the age-model reported in Figure 8c, the base of the section has an age of 6.534 My. This datum is in good agreement with the presence of *Nicklithus amplificus* from the oldest sample, as the inferred age for the First Occurrence (FO) of this species is 6.69 My [62].

The spike of *Discoaster tamalis* occurring in the lowermost part of the section (sample TVCZ-2) has an age of 6.527 My; thus, it cannot correspond to the influx of the species described by Di Stefano et al. [27] at Trave Section with an age of 6.768 My. As already supposed on a biostratigraphic basis, it should represent a further younger influx of the species never before detected.

On the contrary, the influx of *Helicosphaera sellii* occurring in sample TVCZ-14 with an inferred age of 6.429 My, is comparable with the similar event reported in the literature in several Mediterranean sections (Table 1).

The presence of an abundance spike of *D. quinqueramus* in sample TVZC-16 (6.407 My) is noteworthy and may represent a useful tool for stratigraphic correlation.

The almost concomitant presence of abundance spikes of *Sphenolithus* spp., *Helicosphaera* spp., and *G. rotula* defines the so-called "MSC onset event" as defined by Mancini et al. [29,68], here redefined as CN_MSC_OE (=Calcareous Nannofossil MSC Onset Event) (Table 3). In the TCVZ section, the base of this event corresponds to the *Sphenolithus* spp. peak occurring in sample TVCZ-23 and has an age of 5.997 My, in good agreement with the previous literature. The top of the same events falls within sample TVCZ-53 (5.957 My), which also coincides with the deposition of the CdB and the beginning of the barren interval and, thus, the onset of the MSC in the considered area.

Finally, the abundance spike of *Sphenolithus* spp. and *Helicosphaera* spp. occurring above the barren interval (Figure 3) may be compared with the second *Sphenolithus* Influx reported by Manzi et al. [63] at Fanantello, dated at 5.860 My. Yet, it is not possible to assign an age to this bioevent, as the age-model is not available for this tract of the section.

7.2. Age of Foraminiferal Bioevents in the TVCZ Section

The calculated age of main events preceding the MSC from the astrochronological age-model is discussed here with respect to previous findings from other Mediterranean sections (Table 3).

The main events are chronologically listed as follows:

The first abundance influx (FAI) of *T. multiloba* (495 cm, sample TVCZ-14) dated at 6.429 My, generally considered a reliable and synchronous event, fits quite well with previous ages reported by other authors—ranging between 6.40 and 6.415 My.

In the TVCZ section, *N. acostaensis* is relatively abundant from the base; thus, its shift from sinistral to dextral coiling (derived age 6.389 My) is in good agreement with the same event dated at 6.373 Ma at Ain el Beida Section (Morocco) [89] and 6.36 Ma [11] at Sorbas, as well with sx/dx coiling change in *Neogloboquadrinids* at M. dei Corvi—Sardella Section, whose astronomical age is 6.37 My [69].

After the FAI, three other local influxes of *T. multiloba* have been recorded at 670 cm (sample TVCZ-19, 6.377 My), 930 cm (sample TVCZ-26, 6.269 My), and 1095 cm (sample TVCZ-31, 6.209 My). As already published by [11,56], several peaks of *T. multiloba* are recorded between 6.42 My and 6.07 My.

The fourth and last local influx of *T. multiloba*, recorded in the TVCZ section in sample TVCZ-36 (1240 cm) with a derived age of 6.161 My, fits well with a similar event reported by [17,18,56] at 6.17 My. However, after this event, other abundance peaks have been found in younger levels of the Falconara section at 6.09 My and the last one at 6.07 My [56]. Therefore, it is not excluded that younger spikes can be detected in the TVCZ section as well, with a denser sampling resolution towards the CdB. Such influxes are characterized by strictly oligotypic associations, mainly dominated by few genera (e.g., *Turborotalita* and benthic foraminifers of the genera *Bolivina* and *Bulimina*), testifying to cold-eutrophic waters and increase in salinity [1,31,70,76,84]. Although several authors referred to such events for biostratigraphic correlation in the Mediterranean, it should be pointed out that these peaks may have a local significance. Thus, each basin registers salinity variations through time, strictly dependent on local tectonic, climatic, and hydrological changes.

The dominance of dextral *N. acostaensis* is briefly interrupted by a local influx (66%) of sinistral *N. acostaensis* at 855 cm (Table 3). Its age has been astronomically derived at 6.297 My and is quite different from the two already known sinistral influxes of *N. acostaensis*, respectively at 6.13–6.14 My and 6.08–6.09 My [5,11,31,56,70].

The disappearance of planktonic foraminifera, due to the inhospitality of the marine environment, at Torrente Vaccarizzo is preceded by a short barren interval between samples TVCZ-37 and TVCZ-39 (1290–1365 cm), with astrochronological ages of 6.145 to 6.121 My. A similar pattern was already found by Bellanca et al. [6] in the same section. Such an event is not abrupt but rather shows a cyclic transition made of an alternation between barren samples (TVCZ-37, TVCZ-39, and TVCZ-42) and rich association samples (TVCZ-40, TVCZ-43, and TVCZ-44), the result of normal marine influxes within the basin. The definitive disappearance of planktonic foraminifera, in sample TVCZ-46 (1650 cm) at 6.03 My, precedes the "MSC onset bioevent" [29,68] shown by the abundance peak of *Sphenolitus* spp., slightly followed by *H. carteri* s and *G. rotula* spikes. Such an age agrees well with the same event reported by Blanc-Valleron et al. [56] from the Falconara composite section.

8. Conclusions

The main goals deriving from the present study are:

(1) The building of an astrochronology-based age-model for the Messinian pre-evaporitic TVCZ Section. It is based on the abundance variation of *Orbulina* spp. (*Orbulina* peaks), which proved to fit well the 100ky-Eccentricity cycles. This methodology is useful in the absence of other chronostratigraphic constraints, such as magnetostratigraphy and radiometric dating.

(2) Based on the astrochronological age-model, all the collected samples have been dated. Therefore, the age of all recognized bioevents, both nannofossils and foraminifers,

was calculated. Some well-known bioevents were confirmed to be reliable markers for biostratigraphic correlation, and new ones were detected for the first time, improving the biostratigraphic resolution at the MSC onset. In particular, the I *Sphenolitus* + *Helicosphaera* peak (here renamed CN_MSC_OE), with an inferred age of 5.997–5.957 My, represents the last plankton event preceding the CdB deposition. This event is preceded by the disappearance of planktonic foraminifers, which is not abrupt but records an alternation of evaporitic and normal marine phases in the basin.

(3) Many taxa show characteristic "peak-abundance distribution" reflecting stressed conditions in the basin, highlighted by rapid changes in oxygen content, nutrient, salinity, and temperature of the water mass. This trend was already described elsewhere in the stratigraphic levels preceding the MSC.

(4) The age of the MSC onset calculated in the TVCZ section is 5.957 My, in good agreement with previous literature.

Supplementary Materials: The following supporting information can be downloaded at: https://www.mdpi.com/article/10.3390/jmse11050915/s1, Table S1. Samples collected for biostratigraphic analysis in the TVCZ Section and positioned along the reconstructed log. Table S2. Quantitative distribution patterns of calcareous nannofossils and foraminifers at TCVZ Section. Table S3. Quantitative distribution patterns of calcareous nannofossils index taxa at TCVZ Section. Table S4. Planktonic foraminifer assemblage abundances and grade of preservation.

Author Contributions: Conceptualization, A.D.S., R.M. and L.M.F.; field work and sampling: A.D.S., R.M., M.F., S.D., V.B., L.B., Á.N. and N.M.D.; lithostratigraphy: M.F. and S.D.; analysis of calcareous nannofossils: A.D.S., V.B. and N.M.D.; analysis of foraminifers: R.M., A.G.P., M.F. and C.G.; data analysis: M.F. and L.B.; age-models: M.F. and L.M.F.; writing—original draft preparation, A.D.S., R.M. and L.M.F.; writing—review and editing, L.B. and A.G.P.; supervision, A.D.S. and R.M.; funding acquisition, R.M. All authors have read and agreed to the published version of the manuscript.

Funding: University of Catania (UNICT) Grant 2020/2022 (Pia.ce.ri. N. 22725132191) Linea 2, for the following project: "From rifting to continental collision: structural stratigraphic study of the Iblean surface and subsurface, geological and natural heritage of southeastern Sicily" (DATA-SET Resp. R. Maniscalco).

Data Availability Statement: Not applicable.

Acknowledgments: M.F. acknowledges a Ph.D. grant from Catania University.

Conflicts of Interest: The authors declare no conflict of interest.

References

1. Vasiliev, I.; Karakitsios, V.; Bouloubassi, I.; Agiadi, K.; Kontakiotis, G.; Antonarakou, A.; Triantaphyllou, M.; Gogou, A.; Kafousia, N.; Rafélis, M.; et al. Large Sea Surface Temperature, Salinity, and Productivity-Preservation Changes Preceding the Onset of the Messinian Salinity Crisis in the Eastern Mediterranean Sea. *Paleoceanogr. Paleoclimatol.* **2019**, *34*, 182–202. [CrossRef]
2. Antonarakou, A.; Kontakiotis, G.; Vasilatos, C.; Besiou, E.; Zarkogiannis, S.; Drinia, H.; Mortyn, P.G.; Tsaparas, N.; Makri, P.; Karakitsios, V. Evaluating the effect of marine diagenesis on Late Miocene pre-evaporitic sedimentary successions of eastern Mediterranean Sea. *IOP Conf. Ser. Earth Environ. Sci.* **2019**, *221*, 012051. [CrossRef]
3. Pellegrino, L.; Dela Pierre, F.; Natalicchio, M.; Carnevale, G. The Messinian diatomite deposition in the Mediterranean region and its relationships to the global silica cycle. *Earth-Sci. Rev.* **2018**, *178*, 154–176. [CrossRef]
4. Zachariasse, W.J.; Kontakiotis, G.; Lourens, L.J.; Antonarakou, A. The Messinian of Agios Myron (Crete, Greece): A key to better understanding diatomite formation south of Crete, on Gavdos Island. *Palaeogeogr. Palaeoclim. Palaeoecol.* **2021**, *581*, 110633. [CrossRef]
5. Hilgen, F.J.; Krijgsman, W. Cyclostratigraphy and astrochronology of the Tripoli diatomite formation (pre-evaporite Messinian, Sicily, Italy). *Terra Nova* **1999**, *11*, 16–22. [CrossRef]
6. Bellanca, A.; Caruso, A.; Ferruzza, G.; Neri, R.; Rouchy, J.M.; Sprovieri, M.; Blanc-Valleron, M.M. Transition from marine to hypersaline conditions in the Messinian Tripoli Formation from the marginal areas of the central Sicilian Basin. *Sediment. Geol.* **2001**, *140*, 87–105. [CrossRef]
7. Nádudvari, Á.; Forzese, M.; Maniscalco, R.; Di Stefano, A.; Misz-Kennan, M.; Marynowski, L.; Krzykawski, T.; Simoneit, B.R.T. The transition toward the Messinian evaporites identified by biomarker records in the organic-rich shales of the Tripoli Formation (Sicily, Italy). *Int. J. Coal Geol.* **2022**, *260*, 104053. [CrossRef]

8. Kontakiotis, G.; Besiou, E.; Antonarakou, A.; Zarkogiannis, S.D.; Kostis, A.; Mortyn, P.G.; Moissette, P.; Cornée, J.-J.; Schulbert, C.; Drinia, H.; et al. Decoding Sea surface and paleoclimate conditions in the eastern Mediterranean over the Tortonian-Messinian transition. *Palaeogeogr. Palaeoclimatol. Palaeoecol.* **2019**, *534*, 109312. [CrossRef]
9. Kontakiotis, G.; Butiseaca, G.-A.; Karakitsios, V.; Antonarakou, A.; Zarkogiannis, S.; Agiadi, K.; Krsnik, E.; Besiou, E.; Zachariasse, J.-W.; Lourens, L.; et al. Hypersalinity accompanies tectonic restriction in the eastern Mediterranean prior to the Messinian Salinity Crisis. *Palaeogeogr. Palaeoclim. Palaeoecol.* **2022**, *592*, 110903. [CrossRef]
10. Butiseaca, G.A.; van der Meer, M.T.J.; Kontakiotis, G.; Agiadi, K.; Thivaiou, D.; Besiou, E.; Antonarakou, A.; Mulch, A.; Vasiliev, I. Multiple crises preceded the Mediterranean Salinity Crisis: Aridification and vegetation changes revealed by biomarkers and stable isotopes. *Glob. Planet. Chang.* **2022**, *217*, 103951. [CrossRef]
11. Sierro, F.J.; Hilgen, F.J.; Krijgsman, W.; Flores, J.A. The Abad composite (SE Spain): A Messinian reference section for the Mediterranean and the APTS. *Palaeogeogr. Palaeoclim. Palaeoecol.* **2001**, *168*, 141–169. [CrossRef]
12. Flores, J.A.; Sierro, F.J.; Filippelli, G.M.; Bárcena, M.A.; Pérez-Folgado, M.; Vázquez, A.; Utrilla, R. Surface water dynamics and phytoplankton communities during deposition of cyclic late Messinian sapropels sequences in the western Mediterranean. *Mar. Micropaleontol.* **2005**, *56*, 50–79. [CrossRef]
13. Rossignol-Strick, M. Mediterranean Quaternary sapropels, an immediate response of the African monsoon to variation of insolation. *Palaeogeogr. Palaeoclim. Palaeoecol* **1985**, *49*, 237–263. [CrossRef]
14. Hilgen, F.J. Astronomical calibration of Gauss to Matuyama sapropels in the Mediterranean and implication for the Geomagnetic Polarity Time Scale. *Earth Planet. Sci. Lett.* **1991**, *104*, 226–244. [CrossRef]
15. Sierro, F.J.; Flores, J.A.; Zamarreño, I.; Vázquez, A.; Utrilla, R.; Francés, G.; Hilgen, F.J.; Krijgsman, W. Messinian pre-evaporite sapropels and precession-induced oscillations in western Mediterranean climate. *Mar. Geol.* **1999**, *153*, 137–146. [CrossRef]
16. Hilgen, F.J.; Krijgsman, W.; Langereis, C.G.; Lourens, L.J.; Santarelli, A.; Zachariasse, W.J. Extending the astronomical (polarity) time scale into the Miocene. *Earth Planet. Sci. Lett.* **1995**, *136*, 495–500. [CrossRef]
17. Sprovieri, R.; Di Stefano, E.; Sprovieri, M. High resolution chronology for late Miocene Mediterranean stratigraphic events. *Riv. Ital. Paleontol. Stratigr.* **1996**, *102*, 77–104.
18. Sprovieri, R.; Di Stefano, E.; Caruso, A.; Bonomo, S. High resolution stratigraphy in the Messinian Tripoli Formation in Sicily. *Paleopelagos* **1996**, *6*, 415–435.
19. Krijgsman, W.; Hilgen, F.J.; Langereis, C.G.; Santarelli, A.; Zachariasse, W.J. Late Miocene magnetostratigraphy, biostratigraphy and cyclostratigraphy in the Mediterranean. *Earth Planet. Sci. Lett.* **1995**, *136*, 475–494. [CrossRef]
20. Schenau, S.J.; Antonarakou, A.; Hilgen, F.J.; Lourens, L.J.; Nijenhuis, I.A.; Van der Weijden, C.H.; Zachariasse, W.J. Organic-rich layers in the Metochia section (Gavdos, Greece): Evidence for a single mechanism of sapropel formation during the past 10 My. *Mar. Geol.* **1999**, *153*, 117–135. [CrossRef]
21. Pérez-Folgado, M.; Sierro, F.J.; Bàrcena, M.A.; Flores, J.A.; Vàsquez, A.; Utrilla, R.; Hilgen, F.J.; Krijgsman, W.; Filippelli, G.M. Western versus eastern Mediterranean paleoceanographic response to astronomical forcing: A high-resolution microplankton study of precession-controlled sedimentary cycles during the Messinian. *Palaeogeogr. Palaeoclim. Palaeoecol.* **2003**, *190*, 317–334. [CrossRef]
22. Sierro, F.J.; Flores, J.A.; Francés, G.; Vazquez, A.; Utrilla, R.; Zamarreno, I.; Erlenkeuser, H.; Barcena, M.A. Orbitally controlled oscillations in planktic communities and cyclic changes in western Mediterranean hydrography during the Messinian. *Palaeogeogr. Palaeoclim. Palaeoecol.* **2003**, *190*, 289–316. [CrossRef]
23. Pedley, H.M.; Grasso, M. Controls on faunal and sediment cyclicity within the Tripoli and Calcare di Base basins (Late Miocene) of central Sicily. *Palaeogeogr. Palaeoclim. Palaeoecol.* **1993**, *105*, 337–360. [CrossRef]
24. Pedley, H.M.; Grasso, M. A model for the Late Miocene reef-Tripolaceous associations of Sicily and its relevance to aberrant coral growth-forms and reduced biological diversity within the Palaeomediterranean. *Géologie Méditerranéenne* **1994**, *21*, 109–121. [CrossRef]
25. Pedley, H.M.; Maniscalco, R. Lithofacies and faunal succession (faunal phase analysis) as a tool in unravelling climatic and tectonic signals in marginal basins; Messinian (Miocene), Sicily. *J. Geol. Soc.* **1999**, *156*, 855–863. [CrossRef]
26. Suc, J.P.; Violanti, D.; Londeix, L.; Poumot, C.; Robert, C.; Clauzon, G.; Gautier, F.; Turon, J.L.; Ferrier, J.; Chikhi, H.; et al. Evolution of the Messinian Mediterranean environments: The Tripoli Formation at Capodarso (Sicily, Italy). *Rev. Palaeobot. Palynol.* **1995**, *87*, 51–79. [CrossRef]
27. Di Stefano, A.; Verducci, M.; Lirer, F.; Ferraro, L.; Iaccarino, S.M.; Hüsing, S.K.; Hilgen, F.J. Paleoenvironmental conditions preceding the Messinian Salinity Crisis in the Central Mediterranean: Integrated data from the Upper Miocene Trave section (Italy). *Palaeogeogr. Palaeoclim. Palaeoecol.* **2010**, *297*, 37–53. [CrossRef]
28. Riforgiato, F.; Foresi, L.M.; Aldinucci, M.; Mazzei, R.; Donia, F.; Gennari, R.; Salvatorini, G.; Sandrelli, F. Foraminiferal record and astronomical cycles: An example from the Messinian pre-evaporitic Gello Composite Section (Tuscany, Italy). *Stratigraphy* **2008**, *5*, 265–280.
29. Mancini, A.M.; Gennari, R.; Natalicchio, M.; Dela Pierre, F.; Carnevale, G.; Pastero, L.; Pellegrino, L.; Pilade, F.; Lozar, F. Taphonomic bias on calcareous micro and nannofossils and paleoenvironmental evolution across the Messinian Salinity Crisis onset: Insights from the Sorbas Basin (SE Spain). *Palaeogeogr. Palaeoclim. Palaeoecol.* **2022**, *599*, 111056. [CrossRef]

30. Moissette, P.; Cornee, J.-J.; Antonarakou, A.; Kontakiotis, G.; Drinia, H.; Koskeridou, E.; Tsourou, T.; Agiadi, K.; Karakitsios, V. Palaeoenvironmental changes at the Tortonian/Messinian boundary: A deep-sea sedimentary record of the eastern Mediterranean Sea. *Palaeogeogr. Palaeoclim. Palaeoecol.* **2018**, *505*, 217–233. [CrossRef]
31. Karakitsios, V.; Roveri, M.; Lugli, S.; Manzi, V.; Gennari, R.; Antonarakou, A.; Triantaphyllou, M.; Agiadi, K.; Kontakiotis, G.; Kafousia, N.; et al. A Record of the Messinian Salinity Crisis in the Eastern Ionian Tectonically Active Domain (Greece, Eastern Mediterranean). *Basin Res.* **2017**, *29*, 203–233. [CrossRef]
32. Butler, R.W.H.; Grasso, M. Tectonic controls on base-level variations and depositional sequences within thrust-top and foredeep basins: Examples from the Neogene thrust belt of central Sicily. *Basin Res.* **1993**, *5*, 137–151. [CrossRef]
33. Butler, R.W.H.; Lickorish, W.H.; Grasso, M.; Pedley, H.M.; Ramberti, L. Tectonics and sequence stratigraphy in Messinian basins, Sicily: Constraints on the initiation and termination of the Mediterranean salinity crisis. *GSA Bull.* **1995**, *107*, 425–439. [CrossRef]
34. Grasso, M. The Apenninic-Maghrebian orogen in southern Italy, Sicily and adjacent areas. *Anat. Orogen Apennines Adjac. Mediterr. Basins* **2001**, *343*, 255–286. [CrossRef]
35. Elter, P.; Grasso, M.; Parotto, M.; Vezzani, L. Structural setting of the Apennine-Maghrebian thrust belt. *Epis. J. Int. Geosci.* **2003**, *26*, 205–211. [CrossRef]
36. Butler, R.W.H.; Maniscalco, R.; Sturiale, G.; Grasso, M. Stratigraphic variations control deformation patterns in evaporite basins: Messinian examples, onshore and offshore Sicily (Italy). *J. Geol. Soc. Lond.* **2015**, *172*, 113–124. [CrossRef]
37. Ogniben, L. Sedimenti halitico-calcitici a struttura grumosa nel Calcare di Base Messiniano in Sicilia. *G. Geol.* **1963**, *31*, 509–542.
38. Roveri, M.; Bertini, A.; Cosentino, D.; Di Stefano, A.; Gennari, R.; Gliozzi, E.; Grossi, F.; Iaccarino, S.M.; Lugli, S.; Manzi, V.; et al. A high-resolution stratigraphic framework for the latest Messinian events in the Mediterranean area. *Stratigraphy* **2008**, *5*, 327–345.
39. Perri, E.; Gindre-Chanu, L.; Caruso, A.; Cefalà, M.; Scopelliti, G.; Tucker, M. Microbial-mediated pre-salt carbonate deposition during the Messinian salinity crisis (Calcare di Base fm., Southern Italy). *Mar. Pet. Geol.* **2017**, *88*, 235–250. [CrossRef]
40. Natalicchio, M.; Dela Pierre, F.; Birgel, D.; Brumsack, H.; Carnevale, G.; Gennari, R.; Gier, S.; Lozar, F.; Pellegrino, L.; Sabino, M.; et al. Paleoenvironmental change in a precession-paced succession across the onset of the Messinian salinity crisis: Insight from element geochemistry and molecular fossils. *Palaeogeogr. Palaeoclim. Palaeoecol.* **2019**, *518*, 45–61. [CrossRef]
41. Rouchy, J.M.; Caruso, A. The Messinian salinity crisis in the Mediterranean basin: A reassessment of the data and an integrated scenario. *Sediment. Geol.* **2006**, *188*, 35–67. [CrossRef]
42. Caruso, A.; Pierre, C.; Blanc-Valleron, M.-M.; Rouchy, J.M. Carbonate deposition and diagenesis in evaporitic environments: The evaporative and sulphur-bearing limestones during the settlement of the Messinian Salinity Crisis in Sicily and Calabria. *Palaeogeogr. Palaeoclim. Palaeoecol.* **2015**, *429*, 136–162. [CrossRef]
43. Roveri, M.; Manzi, V.; Lugli, S.; Schreiber, B.C.; Caruso, A.; Rouchy, J.M.; Iaccarino, S.M.; Gennari, R.; Vitale, F.P. Clastic vs. primary precipitated evaporites in the messinian sicilian basins. R.C.M.N.S. International Congress "The Messinian salinity crisis revisited II", Parma. Post-congress Field-trip. *Acta Nat. De L'ateneo Parm.* **2006**, *42*, 125–199.
44. Roveri, M.; Flecker, R.; Krijgsman, W.; Lofi, J.; Lugli, S.; Manzi, V.; Sierro, F.J.; Bertini, A.; Camerlenghi, A.; De Lange, G.; et al. The Messinian Salinity Crisis: Past and future of a great challenge for marine sciences. *Mar. Geol.* **2014**, *352*, 25–58. [CrossRef]
45. Manzi, V.; Lugli, S.; Lucchi, F.R.; Roveri, M. Deep-water clastic evaporites deposition in the Messinian Adriatic foredeep (northern Apennines, Italy): Did the Mediterranean ever dry out? *Sedimentology* **2005**, *52*, 875–902. [CrossRef]
46. Manzi, V.; Lugli, S.; Roveri, M.; Schreiber, B.C.; Gennari, R. The Messinian 'Calcare di Base' (Sicily, Italy) revisited. *GSA Bull.* **2011**, *123*, 347–370. [CrossRef]
47. Ryan, W.B.F.; Cita, M.B. The nature and distribution of Messinian erosional surfaces—Indicators of a several-kilometer-deep Mediterranean in the Miocene. *Mar. Geol.* **1978**, *27*, 193–230. [CrossRef]
48. Manzi, V.; Lugli, S.; Roveri, M.; Schreiber, B.C. A new facies model for the Upper Gypsum of Sicily (Italy): Chronological and palaeontological constraints for the Messinian salinity crisis in the Mediterranean. *Sedimentology* **2009**, *56*, 1937–1960. [CrossRef]
49. Decima, D.; Wezel, F.C. Late Miocene evaporites of the central Sicilian Basin, Italy. *Initial. Rep. Deep. Sea Drill. Proj.* **1973**, *13*, 1234–1241. [CrossRef]
50. Maniscalco, R.; Casciano, C.I.; Distefano, S.; Grossi, F.; Di Stefano, A. Facies Analysis in the Second Cycle Messinian Evaporites Predating the Early Pliocene Reflooding: The Balza Soletta Section (Corvillo Basin, Central Sicily). *Ital. J. Geosci.* **2019**, *138*, 301–316. [CrossRef]
51. Butler, R.W.H.; Grasso, M.; Gardiner, W.; Sedgeley, D. Depositional patterns and their tectonic controls within the Plio-Quaternary carbonate sands and muds of onshore and offshore SE Sicily (Italy). *Mar. Pet. Geol.* **1997**, *14*, 879–892. [CrossRef]
52. Butler, R.W.H.; Lickorish, W.H. Using high-resolution stratigraphy to date fold and thrust activity: Examples from the Neogene of south-central Sicily. *J. Geol. Soc.* **1997**, *154*, 633–643. [CrossRef]
53. Zecchin, M.; Catuneanu, O. High-resolution sequence stratigraphy of clastic shelves VI: Mixed siliciclastic-carbonate systems. *Mar. Pet. Geol.* **2017**, *88*, 712–723. [CrossRef]
54. Sturiale, G.; Maniscalco, R.; De Guidi, G.; Pedley, H.M.; Grasso, M. Carta geologica dei Bacini di Corvillo e Mandre (Sicilia centrale). Scala 1:50.000. *Ital. J. Geosci.* **2010**, *129*, 316–326. [CrossRef]
55. Grasso, M.; Pedley, H.M.; Romeo, M. The Messinian Tripoli Formation of northcentral Sicily: Palaeoenvironmental interpretations based on sedimentological, micropalaeontological and tectonic studies. *Paleobiol. Cont. Montp.* **1990**, *17*, 189–204.

56. Blanc-Valleron, M.M.; Pierre, C.; Caulet, J.P.; Caruso, A.; Rouchy, J.M.; Cespuglio, G.; Sprovieri, R.; Pestrea, S.; Di Stefano, E. Sedimentary, stable isotope and micropaleontological records of paleoceanographic change in the Messinian Tripoli Formation (Sicily, Italy). *Palaeogeogr. Palaeoclim. Palaeoecol.* **2002**, *185*, 255–286. [CrossRef]
57. Bown, P.R.; Young, J. Calcareous Nannofossil Biostratigraphy. In *British Micropaleontological Society Publication Series*; Bown, P.R., Ed.; Springer Science+ Business Media, LLC: New York, NY, USA, 1998; pp. 1–15.
58. Di Stefano, A.; Baldassini, N.; Raffi, I.; Fornaciari, E.; Incarbona, A.; Negri, A.; Bonomo, S.; Villa, G.; Di Stefano, E.; Rio, D. Neogene-Quaternary Mediterranean Calcareous Nannofossil Biozonation and Biochronology. *Stratigraphy* **2023**. *submitted*.
59. Lirer, F.; Foresi, L.M.; Iaccarino, S.M.; Salvatorini, G.; Turco, E.; Cosentino, C.; Sierro, F.J.; Caruso, A. Mediterranean Neogene planktonic foraminifer biozonation and biochronology. *Earth-Sci. Rev.* **2019**, *196*, 102869. [CrossRef]
60. Negri, A.; Giunta, S.; Hilgen, F.; Krijgsman, W.; Vai, G.B. Calcareous nannofossil biostratigraphy of the M. del Casino section (northern Apennines, Italy) and paleoceanographic conditions at times of Late Miocene sapropel formation. *Mar. Micropaleontol.* **1999**, *36*, 13–30. [CrossRef]
61. Negri, A.; Villa, G. Calcareous nannofossil biostratigraphy, biochronology and paleoecology at the Tortonian/Messinian boundary of the Faneromeni section (Crete). *Palaeogeogr. Palaeoclim. Palaeoecol.* **2000**, *156*, 195–209. [CrossRef]
62. Raffi, I.; Mozzato, C.A.; Fornaciari, E.; Hilgen, F.J.; Rio, D. Late Miocene calcareous nannofossil biostratigrapy and astrobiochronology for the Mediterranean region. *Micropaleontology* **2003**, *49*, 1–26. [CrossRef]
63. Manzi, V.; Roveri, M.; Gennari, R.; Bertini, A.; Biffi, U.; Giunta, S.; Iaccarino, S.M.; Lanci, L.; Lugli, S.; Negri, A.; et al. The deep-water counterpart of the Messinian Lower Evaporites in the Apennine foredeep: The Fanantello section (Northern Apennines, Italy). *Palaeogeogr. Palaeoclim. Palaeoecol.* **2007**, *251*, 470–499. [CrossRef]
64. Morigi, C.; Negri, A.; Giunta, S.; Kouwenhoven, T.; Krijgsman, W.; Blanc-Valleron, M.M.; Orszag-Sperber, F.; Rouchy, J.M. Integrated quantitative biostratigraphy of the latest Tortonian-early Messinian Pissouri section (Cyprus): An evaluation of calcareous plankton bioevents. *Geobios* **2007**, *40*, 267–279. [CrossRef]
65. Iaccarino, S.M.; Bertini, A.; Di Stefano, A.; Ferraro, L.; Gennari, R.; Grossi, F.; Lirer, F.; Manzi, V.; Menichetti, E.; Ricci Lucchi, M.; et al. The Trave section (Monte dei Corvi, Ancona, Central Italy): An integrated paleontological study of the Messinian deposits. *Stratigraphy* **2008**, *5*, 283–308.
66. Lozar, F.; Violanti, D.; Bernardi, E.; Dela Pierre, F.; Natalicchio, M. Identifying the onset of the Messinian salinity crisis: A reassessment of the biochronostratigraphic tools (Piedmont Basin, NW Italy). *Newsl. Stratigr.* **2018**, *51*, 11–31. [CrossRef]
67. Lozar, F.; Negri, A. A review of basin-wide calcareous nannofossil bioevents in the Mediterranean at the onset of the Messinian salinity crisis. *Mar. Micropaleontol.* **2019**, *151*, 101752. [CrossRef]
68. Mancini, A.M.; Gennari, R.; Ziveri, P.; Mortyn, P.G.; Stolwijk, D.J.; Lozar, F. Calcareous nannofossil and foraminiferal trace element records in the Sorbas Basin: A new piece of the Messinian Salinity Crisis onset puzzle. *Palaeogeogr. Palaeoclim. Palaeoecol* **2020**, *554*, 109796. [CrossRef]
69. Hüsing, S.K.; Kuiper, K.F.; Link, W.; Hilgen, F.J.; Krijgsman, W. The upper Tortonian–lower Messinian at Monte dei Corvi (Northern Apennines, Italy): Completing a Mediterranean reference section for the Tortonian Stage. *Earth Planet. Sci. Lett.* **2009**, *282*, 140–157. [CrossRef]
70. Drinia, H.; Antonarakou, A.; Tsaparas, N.; Kontakiotis, G. Palaeoenvironmental conditions preceding the Messinian Salinity Crisis: A case study from Gavdos Island. *Geobios* **2007**, *40*, 251–265. [CrossRef]
71. Foresi, L.M.; Baldassini, N.; Sagnotti, L.; Lirer, F.; Di Stefano, A.; Caricchi, C.; Verducci, M.; Salvatorini, G.; Mazzei, R. Integrated stratigraphy of the St. Thomas section (Malta Island): A reference section for the lower Burdigalian of the Mediterranean Region. *Mar. Micropaleontol.* **2014**, *111*, 66–89. [CrossRef]
72. Fabbrini, A.; Baldassini, N.; Caricchi, C.; Foresi, L.M.; Sagnotti, L.; Dinarès-Turell, J.; Di Stefano, A.; Lirer, F.; Menichetti, M.; Winkler, A.; et al. In search of the Burdigalian GSSP: New evidence from the Contessa Section (Italy). *Ital. J. Geosci.* **2019**, *138*, 274–295. [CrossRef]
73. Distefano, S.; Gamberi, F.; Baldassini, N.; Di Stefano, A. Neogene stratigraphic evolution of a tectonically controlled continental shelf: The example of the Lampedusa Island. *Ital. J. Geosci.* **2021**, *138*, 418–431. [CrossRef]
74. Manzi, V.; Gennari, R.; Lugli, S.; Persico, D.; Reghizzi, M.; Roveri, M.B.; Charlotte Schreiber, B.C.; Calvo, R.; Gavrieli, I.; Gvirtzman, Z. The onset of the Messinian salinity crisis in the deep Eastern Mediterranean basin. *Terra Nova* **2018**, *30*, 189–198. [CrossRef]
75. Manzi, V.; Gennari, R.; Hilgen, F.; Krijgsman, W.; Lugli, S.; Roveri, M.; Sierro, F.J. Age refinement of the Messinian salinity crisis onset in the Mediterranean. *Terra Nova* **2013**, *25*, 315–322. [CrossRef]
76. Gennari, R.; Lozar, F.; Natalicchio, M.; Zanella, E.; Carnevale, G.; Pierre, F.D. Chronology of the Messinian events in the northernmost part of the Mediterranean: The Govone section (Piedmont basin, NW Italy). *Riv. Ital. Paleontol. Stratigr.* **2020**, *126*, 2. [CrossRef]
77. Zachariasse, W.J.; Lourens, L.J. The Messinian on Gavdos (Greece) and the status of currently used ages for the onset of the MSC and gypsum precipitation. *Newsl. Stratigr.* **2022**, *55*, 3. [CrossRef]
78. Bé, A.W.H.; Tolderlund, D.S. Distribution and ecology of living planktonic foraminifera in surface waters of the Atlantic and Indian Oceans. In *Micropaleontology of the Oceans*; Funnell, B.M., Riedel, W.R., Eds.; Cambridge University Press: London, UK, 1971; pp. 105–149.
79. Spero, H.J. *Modern Planktonic Foraminifera*; Hemleben, C., Spindler, M., Anderson, O.R., Eds.; Springer: New York, NY, USA, 1989; p. 363.

80. Bijma, J.; Faber, W.W.; Hemleben, C. Temperature and salinity limits for growth and survival of some planktonic foraminifers in laboratory cultures. *J. Foraminifer. Res.* **1990**, *20*, 95–116. [CrossRef]
81. Pujol, C.; Grazzini, C. Distribution patterns of live planktic foraminifers as related to regional hydrology and productive systems of the Mediterranean Sea. *Mar. Micropaleontol.* **1995**, *25*, 187–217. [CrossRef]
82. Zarkogiannis, S.; Kontakiotis, G.; Antonarakou, A. Recent planktonic foraminifera population and size response to Eastern Mediterranean hydrography. *Rev. De Micropaléontologie* **2020**, *69*, 100450. [CrossRef]
83. Kouwenhoven, T.J.; Morigi, C.; Negri, A.; Giunta, S.; Krijgsman, W.; Rouchy, J.M. Paleoenvironmental evolution of the eastern Mediterranean during the Messinian: Constraints from integrated microfossil data of the Pissouri Basin (Cyprus). *Mar. Micropaleontol.* **2006**, *60*, 17–44. [CrossRef]
84. Violanti, D.; Lozar, F.; Natalicchio, M.; Dela Pierre, F.; Bernardi, E.; Clari, P.; Cavagna, S. Stress-tolerant microfossils of a Messinian succession from the Northern Mediterranean basin (Pollenzo section, Piedmont, northwestern Italy). *Boll. Della Soc. Paleontol. Ital.* **2013**, *52*, 45–54. [CrossRef]
85. Brachert, T.C.; Bornemann, A.; Reuter, M.; Galer, S.J.; Grimm, K.I.; Fassoulas, C. Upwelling history of the Mediterranean Sea revealed by stunted growth in the planktic foraminifera Orbulina universa (early Messinian, Crete, Greece). *Int. J. Earth Sci. (Geol. Rundsch.)* **2015**, *104*, 263–276. [CrossRef]
86. Sprovieri, M.; Bellanca, A.; Neri, R.; Mazzola, S.; Bonanno, A.; Bernardo, P.; Sorgent, R. Astronomical calibration of Late Miocene stratigraphic events and analysis of precessionally driven paleoceanographic changes in the Mediterranean Basin. *Soc. Geol. Ital. Mem.* **1999**, *54*, 7–24.
87. Hammer, Ø.; Harper, D.A.T.; Ryan, P.D. PAST: Paleontological Statistics Software Package for Education and Data Analysis. *Palaeontol. Electron.* **2001**, *4*, 9. Available online: http://palaeo-electronica.org/2001_1/past/issue1_01.htm (accessed on 1 March 2023).
88. Laskar, J.; Robutel, P.; Joutel, F.; Gastineau, M.; Correia, A.; Levrard, B. A long-term numerical solution for the insolation quantities of the Earth. *Astron. Astrophys.* **2004**, *428*, 261–285. [CrossRef]
89. Krijgsman, W.; Gaboardi, S.; Hilgen, F.J.; Iaccarino, S.; Kaenel, E.; van der Laan, E. Revised astrochronology for Ain el Beida sectin (Atlantic Morocco): No glacio-eustatic control for the onset of the Messinian Salinity Crisis. *Stratigraphy* **2004**, *1*, 87–101. Available online: http://hdl.handle.net/11381/1844339 (accessed on 1 March 2023).